Draft version February 1, 2008
Preprint typeset using LaTeX style emulateapj v. 10/09/06

arXiv:0708.0835v1 [astro-ph] 7 Aug 2007

REST–FRAME ULTRAVIOLET TO NEAR INFRARED OBSERVATIONS OF AN INTERACTING LYMAN BREAK GALAXY AT $Z = 4.42$

Joshua D. Younger[1], Jia–Sheng Huang[1], Giovanni G. Fazio[1], Thomas J. Cox[1], Kamson Lai[1], Philip F. Hopkins[1], Lars Hernquist[1], Casey J. Papovich[2,3], Luc Simard [4], Lihwai Lin[5,6], Yi–Wen Cheng[7], Haojin Yan[8], Dušan Kereš[1], & Alice E. Shapley[9]

Draft version February 1, 2008

ABSTRACT

We present the rest–frame ultraviolet through near infrared spectral energy distribution for an interacting Lyman break galaxy at a redshift $z = 4.42$, the highest redshift merging system known with clearly resolved tidal features. The two objects in this system – HDF–G4 and its previously unidentified companion – are both B_{435} band dropouts, have similar $V_{606} - i_{775}$ and $i_{775} - z_{850}$ colors, and are separated by $1''$, which at $z = 4.42$ corresponds to 7 kpc projected nuclear separation; all indicative of an interacting system. Fits to stellar population models indicate a stellar mass of $M_\star = 2.6 \times 10^{10} M_\odot$, age of $\tau_\star = 720$ My, and exponential star formation history with an e–folding time $\tau_0 = 440$ My. Using these derived stellar populations as constraints, we model the HDF–G4 system using hydrodynamical simulations, and find that it will likely evolve into a quasar by $z \sim 3.5$, and a quiesent, compact spheroid by $z \sim 2.5$ similar to those observed at $z \gtrsim 2$. And, the existence of such an object supports galaxy formation models in which major mergers drive the high redshift buildup of spheroids and black holes.

Subject headings: cosmology:observations – galaxies:evolution – galaxies: high–redshift – galaxies: stellar content – galaxies: interacting – infrared: galaxies

1. INTRODUCTION

Recently, there have been great advances in understanding the nature and evolution of high–redshift galaxies. Through either color–selection criteria (Steidel et al. 2003; Franx et al. 2003; Daddi et al. 2004), Lyman–α emission (Rhoads & Malhotra 2001; Malhotra & Rhoads 2002; Ajiki et al. 2003; Hu et al. 2004; Taniguchi et al. 2005) or blank–field submillimeter surveys combined with radio observations (Smail et al. 2000; Barger et al. 2000; Ivison et al. 2002; Borys et al. 2003; Chapman et al. 2005; Coppin et al. 2005) observers have compiled large catalogs of $z \gtrsim 2$ galaxies. Subsequent photometric and spectroscopic followup has been successful at constraining the physical properties of these galaxy populations, including the evolution of the star formation rate (SFR) and stellar mass density out to $z \sim 3$ (Shapley et al. 2003; Barmby et al. 2004; Shapley et al. 2005; Lai et al. 2007).

One method for selecting high–redshift galaxies – the Lyman break dropout techinque (Steidel & Hamilton 1993) – uses the 912Å break to select $z \sim 3$ galaxies. Spectroscopic followup has provided substantial samples of confirmed $z \sim 3-4$ galaxies (Steidel et al. 1999, 2003). These Lyman break galaxies (LBGs) are known to have high star formation rates relative to local galaxies of the same stellar mass, as revealed by their high rest frame UV luminosity (Steidel et al. 2003). Until recently, stellar masses for these objects were estimated using ground–based optical photometry. At these wavelengths in the rest–frame, the luminosity is dominated by recent star formation, rather than the accumulated mass from older stellar populations. Studies using the Infrared Array Camera (IRAC: Fazio et al. 2004) on the *Spitzer* Space Telescope, which provides photometry out to 8μm in the observed frame, have used the rest–frame K band luminosity to place more robust constraints on the bulk of the stellar content of LBGs at $z \sim 3$ (Rigopoulou et al. 2006).

At the same time, recent theoretical modeling (Hopkins et al. 2006a,b, 2007a,b) and simulations (Cox et al. 2006) have suggested a link between merging galaxy populations, quasars, and present day ellipticals through the self–regulated growth of supermassive black holes (SMBHs) in gas–rich major mergers (Di Matteo et al. 2005). The presence of large amounts of dust (Sawicki & Yee 1998; Calzetti 2001; Takeuchi & Ishii 2004) that implies a high SFR, in combination with clustering arguments (Adelberger et al. 2005), and a merging fraction of $\sim 10-25\%$ at high redshift (Lotz et al. 2006) have suggested empirically that high–redshift LBGs may be the progenitors of those same present–day ellipticals (Pettini et al. 1998). As a result, major mergers involving LBGs at high redshift may provide observational evidence of a link between these populations.

In this work we present optical through infrared ob-

---

[1] Harvard–Smithsonian Center for Astrophysics, 60 Garden Street, Cambridge, MA 02138, USA
[2] Steward Observatory, University of Arizona, 933 North Cherry Avenue, Tucson, AZ 85721, USA
[3] *Spitzer* Fellow
[4] Herzberg Institute of Astrophysics, National Research Council of Canada, 5071 West Saanich Road, Victoria, BC V9E 2E7, Canada
[5] UCO/Lick Observatory, University of California, 1156 High Street, Santa Cruz, CA 95064, USA
[6] Department of Physics, National Taiwan University, No. 1, Sec. 4., Roosevelt Road, Taipei 106, Taiwan
[7] Institute of Astronomy, National Central University, Chung-li, Taiwan
[8] Carnegie Observatories, 813 Santa Barbara Street, Pasadena, California, 91101 USA
[9] Department of Astrophysical Sciences, Princeton University, Peyton Hall, Ivy Lane, Princeton, NJ 08544

servations of HDF–G4, an LBG with a spectroscopically confirmed redshift of $z = 4.42$ in the Hubble Deep Field North (HDFN) with α(J2000) = 12:37:20.57 and δ(J2000) =+62:11:6.08 from the catalog of Steidel et al. (1999). This object, and its previously unidentified companion, constitute the most distant interacting system observed to date for which the resolved morphology clearly suggests a merger. In § 2, we present multiwavelength data for the HDF–G4 system. From these data, in § 3, we use stellar population synthesis models to derive stellar masses and star formation rates (SFRs) for each component. In § 4, we use the observed stellar populations and morpholgy to constrain a model of the HDF–G4 system using hydrodynamical simulations. Finally, in § 5, we discuss the implications of the predictions of our model for the future evolution of the HDF–G4 system. Our analysis suggests that HDF–G4 will be a high–redshift passive spheroid by $z \sim 2.5$, similar to those observed by Labbé et al. (2005) and Zirm et al. (2007). For the proceeding analysis, we assume the concordance cosmological model; a flat ΛCDM cosmology with $\Omega_\Lambda = 0.7$ and $h = 0.7$. All magnitudes presented are in the AB system.

2. MULTI-WAVELENGTH PHOTOMETRY OF HDF-G4

The Great Observatories Origins Deep Survey (GOODS), which includes the HDFN, is the deepest multi-wavelength survey, detecting galaxies at extremely high redshifts in optical and IR bands (Mobasher et al. 2005; Yan et al. 2006; Lai et al. 2007), and potentially interacting systems at very high redshift at $z \gtrsim 4$ (Rhoads et al. 2005; Yan et al. 2005). The wealth of multi–wavelength data available for GOODS fields, from the X–Ray to radio, makes it ideal for studying the properties of such interesting systems.

We visually inspected the available optical imaging data, and find that HDF-G4 appears to be one object in the ground–based Subaru images (Capak et al. 2004), but is resolved into two objects in the ACS mosaic (Giavalisco et al. 2004). Aperture photometry obtained with SEXTRACTOR, a publicly available source detection and photometry package (Bertin & Arnouts 1996), for both the primary (C1) and secondary (C2) components were taken from the public catalog for all four ACS mosaics: F435W (B_{435}), F606W (V_{606}), F775W (i_{775}), and F850LP (z_{850}). C2 is 1 magnitude fainter in the ACS i_{775} band, and $\sim 1''$ away from C1. Furthermore, the position angle and center of the slit–mask indicate that the observed optical spectrum is of C1 only.

There are three pieces of evidence suggesting that C1 and C2 are physically associated with each other. The first is that both objects are B_{435} dropouts with similar observed optical colors, indicating that they are at comparable redshift. The second is their relative angular separation, which at $z = 4.42$ corresponds to a projected internuclear distance of 7 kpc. This is similar to local interacting systems such as the "Antennae" (Whitmore & Schweizer 1995), II ZW 96 (Goldader et al. 1997), or ultraluminous infrared galaxies (ULIRGs; Rigopoulou et al. 1999; Surace et al. 2000). The third, and most compelling piece of evidence is a material bridge connecting both components. This feature is low surface brightness – typically no more than 2σ above the sky noise per pixel – but highly statistically significant; a Monte–Carlo analysis indicates that it is detected at 10σ in the stacked optical image (see Figure 1). It furthermore has similar colors to C1 and C2, and is not detected in B_{435} (see Table 1).

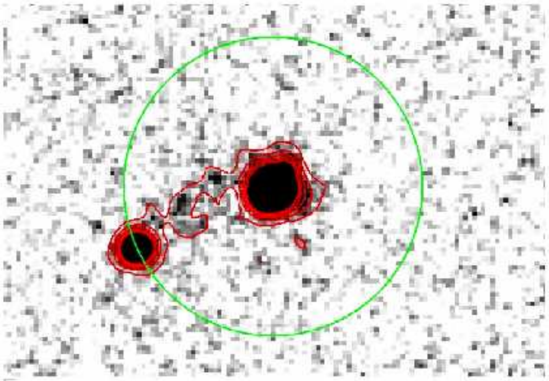

FIG. 1.— Stacked optical imaging data centered on HDF–G4 for all four ACS filters: B_{435}, V_{606}, i_{775}, and z_{850}. Red contours correspond to 2–5 standard deviations above the noise. The green circle has a $1''$ radius, which at this redshift corresponds to ~ 7 kpc in our assumed cosmology. Note the material exchanged between the two sources, contained within a 2–σ contour. This is, despite its low per–pixel surface brightness, a highly statistically significant feature that indicates an interacting system.

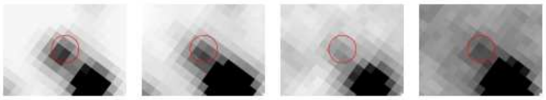

FIG. 2.— Infrared imaging data, with negative contrast, centered on HDF–G4, in all four IRAC channels: (left to right) 3.6, 4.5, 5.8, and 8.0 μm. The red circles have a $1''$ radius. HDF–G4 is clearly detected at 3.6μm and 4.5μm , and marginally detected at 5.8μm and 8.0μm .

This system is also marginally detected in the CFHT WIRCam J and K band images (Lin 2006, Simard 2006, private communication). The centroid of the K-band counterpart is $0.35''$ offset from C1, but $0.8''$ from C2. Given the $0.9''$ seeing in the J and K images, we argue the detected J- and K-band flux is dominated by C1.

The GOODS IRAC image is very deep, and thus both C1 and C2 should be detected at least at 3.6 and 4.5μm. Indeed, we find significant detections at 3.6 and 4.5μm, and marginal detections at 5.8 and 8.0μm (see Figure 2). We obtain aperture photometry (see Table 1) for HDF–G4, after subtracting out bright neighbors to minimize contamination using STARFINDER, a publically available PSF–fitting photometry package (Diolaiti et al. 2000). Errors were estimated using a Monte–Carlo analysis. IRAC, however, has $2.1''$ resolution, and thus cannot resolve C1 and C2. We use the z_{850} flux ratio to estimate the C2 contribution to the total IRAC flux of this system. C2 has a somewhat bluer color with $V_{606} - z_{850} = 0.64$, as compared to C1 with $V_{606} - z_{850} = 1.09$. This is very similar to a merging system at z=3.01 found by Huang et al. (2006), in which the IR flux densities are dominated by the red luminous component. We argue that C2 should also have bluer $z_{850} - [3.6]$ color than C1, and use the z_{850} flux ratio to estimate an upper limit of 10% on the contribution of C2 to the unresolved IRAC flux densities.

The HDFN was additionally covered by the Very Large Array at 1.4 GHz to a depth of 40 μJy (Richards 2000),

.

TABLE 1
Photometry of Different Components of the HDF–G4 System

	B_{435} [mag]	V_{606} [mag]	i_{775} [mag]	z_{850} [mag]	J [mag]	K_s [mag]	3.6μm [μJy]	4.5μm [μJy]	5.8μm [μJy]	8.0μm [μJy]
C1	> 27.2	25.87 ± 0.02	24.72 ± 0.02	24.77 ± 0.02	23.65 ± 0.59	23.59 ± 0.18	1.34 ± 0.22	0.92 ± 0.34	0.68 ± 3.47	0.79 ± 0.94
C2	> 27.2	26.43 ± 0.03	25.67 ± 0.03	25.80 ± 0.04	...	...	...	...	...	...
Bridge[a]	> 27.74	27.92 ± 0.19	26.78 ± 0.12	26.72 ± 0.15	...	...	...	...	...	...

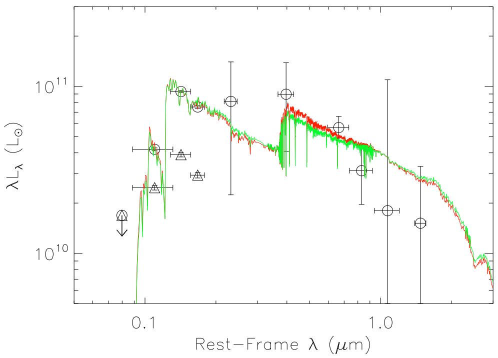

Fig. 3.— The SED of HDF–G4 (open circles) and its companion (open triangles) from the rest–frame UV to the NIR, along with the best–fit Bruzual & Charlot (2003) stellar population synthesis models for an exponential (red; ESF) and continuous (green; CSF) star formation history. IRAC data for 5.8μm and 8.0μm are shown for completeness, but are excluded from the fitting because of their low significance.

MIPS to a depth of $\sim 70\mu$Jy at 24μm , and the *Chandra* X–Ray Telescope to depths of 2.5×10^{-17} and 1.4×10^{-16} erg cm^{-2} in the soft (0.5-2.0 keV) and hard (2-10 keV) bands respectively (Alexander et al. 2003). There was, however, no detection of either HDF–G4 or its companion in the publicly released source lists or imaging data. This is all consistent – and in particular the lack of 24μm or 1.4 GHz emission – with the high redshift of HDF–G4.

We present the spectral energy distribution (SED) of HDF–G4 (open circles) and and its companion (open triangles), along with best fit models (see § 3) in Figure 3. All the available photometry for C1, C2, and the bridge are presented in Table 1.

3. ANALYSIS OF THE STELLAR POPULATIONS

Our observations of each component of the HDF–G4 system can be used to constrain the underlying stellar population at the time of our observations. To estimate the age and mass of the stellar population of the primary component of HDF–G4 (C1), we fit its SED to a grid of population synthesis models (Bruzual & Charlot 2003), assuming a Salpeter (1955) IMF, with three different parameterized star formation histories: a single stellar population (SSP) instantaneous burst, continuous star formation (CSF), and an exponential decay τ–model (ESF). We consider solar and sub–solar ($Z_\odot/200$) models, in addition to including the effects of Calzetti et al. (2000) dust extinction and Madau (1995) Lyman–α forest absorption. Our fits exclude observations in IRAC Channels 3 and 4, which are poorly constrained by the measurement.

Results for the best–fit CSF and ESF models are shown in Figure 3; the SSP models were excluded because they were both a poor fit to the data. Requiring the age of the stellar population $\tau_\star$ to be less than a Hubble time at $z = 4.42$ further excludes the sub–solar CSF and ESF models. The best fit overall, with χ^2/d.o.f. $= 1.46$ was the solar metallicity ESF model, with e–folding time $\tau_0 = 440$ My, stellar age $\tau_\star = 720$ Myr, stellar mass $M_\star = 2.6 \times 10^{10} M_\odot$, and dust extinction $E(B-V) = 0$. The best–fit CSF model, with χ^2/d.o.f. $= 2.24$, had $\tau_\star = 1020$ Myr, $M_\star = 2.6 \times 10^{10} M_\odot$, $E(B-V) = 0.05$, and star formation rate SFR $= 32\ M_\odot$ yr^{-1} . These results are somewhat sensitive to the choice of IMF; e.g., assuming a Chabrier (2003) distribution will reduce the inferred stellar masses by $\sim 30-40\%$. These inferred stellar masses and SFRs are broadly consistent with studies applying a similar analysis to large populations of LBGs (Papovich et al. 2001; Shapley et al. 2001), and with 8μm selected LBGs with similar infrared–to–optical colors at $z \sim 3$ (Rigopoulou et al. 2006). We note that our best fit stellar populations indicate minimal dust extinction, which is unusual for LBGs but is consistent with the least obscured objects at $z \sim 2-3$ (Papovich et al. 2001; Shapley et al. 2001).

We do not have sufficient spectral coverage to fit models to the photometry for C2 or the bridge. However, at $z = 4.42$, the observed optical images cover the rest–frame ultraviolet continuum from 800-2310Å. The integrated spectrum in this waveband is dominated by young stars, and therefore scales linearly with the star formation rate (Kennicutt 1998; Madau et al. 1998). Using the calibrations of Kennicutt (1998) for the intrinsic luminosity at 1500 Å, which assume CSF and a Salpeter (1955) IMF, we find that our i_{775} (rest–frame $\lambda_{eff} \approx 1421$Å) photometry implies SFR $\approx 9\ M_\odot$ yr^{-1} . Similarly, the bridge traces significant off–nuclear star formation, with SFR $\approx 3\ M_\odot$ yr^{-1} as inferred from the i_{775} magnitude. If a Scalo (1986) IMF is used, these estimates increase by a factor of ~ 2.

The lack of a detection of HDF–G4 in deep *Chandra* observations can constrain the relative contributions of an active galactic nucleus (AGN) and stellar components of the bolometric luminosity in C1. From the AGN SED template of Hopkins et al. (2007d), we find that the limiting flux of the hard band ($2-8$ keV) puts a strict upper limit, in the absence of significant scattering or absorption by dust, of $L_{AGN} \lesssim 2 \times 10^{10} L_\odot$ on the bolometric AGN luminosity. We believe that neglecting the effects of dust on the emitted X–rays is a good approximation for two reasons: the population synthesis fits indicate that there is little dust attenuation in the optical, and at $z = 4.42$ the *Chandra* hard band probes very hard X–rays ($11-44$ keV) that are largely unaffected by dust in the line of sight. The integrated intrinsic stellar luminosity, from the best–fit ESF model, is $L_{stars} = 2.0 \times 10^{11} L_\odot$, which constrains the ratio of the luminosity of the AGN to the stellar component of HDF–G4 to $L_{AGN}/L_{stars} \lesssim 0.1$; C1 is clearly starburst

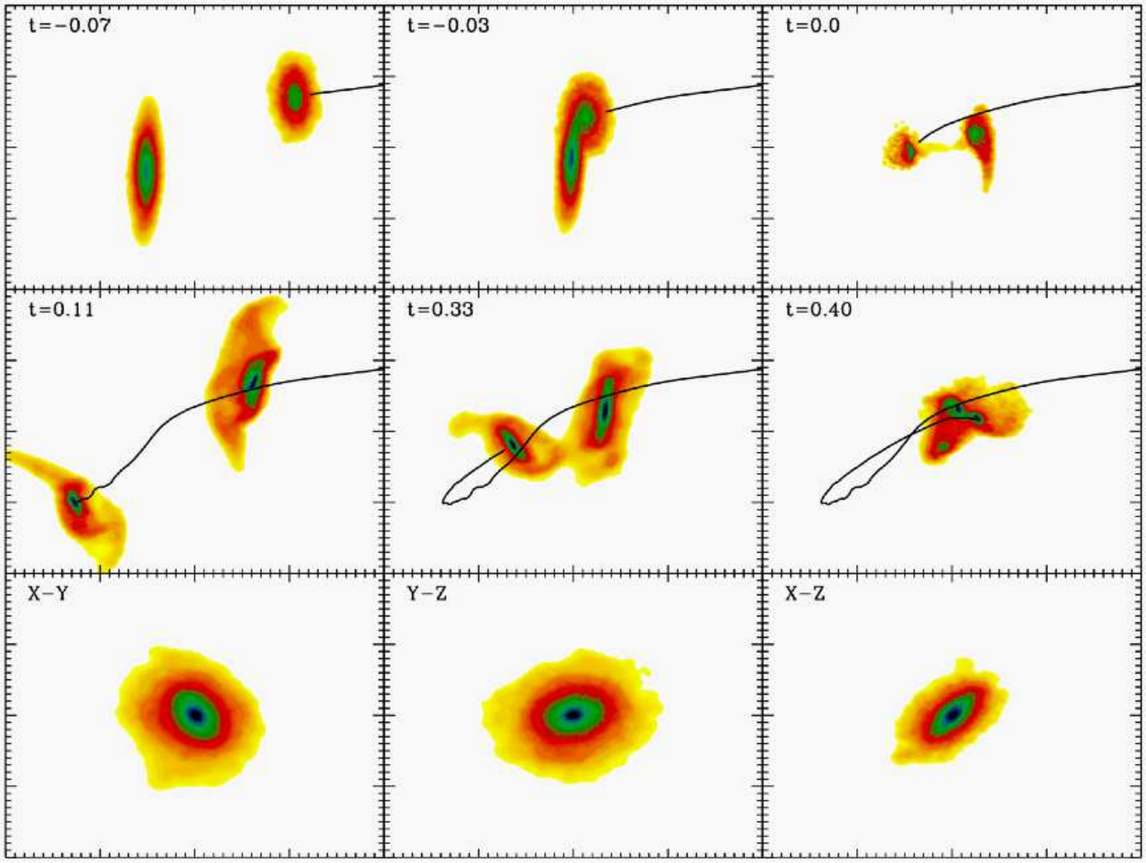

FIG. 4.— Schematic of the merger simulation that best matches our observations. The top six panels show the stellar surface mass density looking down on the orbital plane. They are 60 h^{-1} kpc on a side , the time relative to the start of the simulation in h^{-1} Gyr is given in the upper right hand corner, and the black curve shows the path of the center of the smaller component (C2). The bottom three panels show the remnant spheroid viewed from three different projections.

dominated.

4. COMPARISON TO HYDRODYNAMICAL SIMULATION

In order to gain some insight into the nature of the HDF–G4 system, we have employed hydrodynamic simulations and designed a model for the encounter. Our simulations were preformed using an updated version of the publicly available N–Body/SPH (Smoothed Particle Hydrodynamics) code GADGET2 (Springel 2005). They include star formation, supernova feedback, and black hole accretion; for a detailed description of our methodology, see Springel et al. (2005a,b). Using this code, we track the interaction and merger of two disk galaxies whose properties are scaled, as in Robertson et al. (2006), to be appropriate for a redshift of $z = 5$.

The progenitor galaxy models are motivated by the stellar mass and size of the observed components of the HDF–G4 system. In particular, the observed relative fluxes of C1 and C2, assuming a constant M/L ratio, imply a 2:1 interaction. This is reproduced with progenitor disks initialized with circular velocities of $V_{200} = 320$ and 200 km s^{-1} respectively, where V_{200} is the Keplerian circular velocity at a mean overdensity of $200\rho_c$. Both models have baryon fractions of 5% and initial gas fractions of $f_g = 0.8$, which is consistent with gas fractions observed in $z \gtrsim 2$ disks (Erb et al. 2006), and is further motivated by models (Hopkins et al. 2007c) to explain large black hole to host stellar mass ratios at $z \gtrsim 2$ (Peng et al. 2006). They are realized with 10^6 and 5×10^5 dark matter, and 1.2×10^5 and 6×10^4 baryonic particles respectively.

Our high redshift merger model assumes that HDF–G4 is witnessed soon after the first passage of the two galaxies. This is based on the appreciable projected physical separation that implies a lower limit of 7 kpc on the internuclear distance, regular appearance, and bridge of material that connects the two components. The bridge in particular, while potentially reflective of the irregular rest–frame UV morphology of star–forming systems (e.g., Law et al. 2007), is also a characteristic feature of galaxy interactions at low redshift and provides the strongest constraints on the mutual orbit. A prograde encounter for either galaxy can be ruled out based upon the absence of the symmetric tidal features that these interactions produce. More likely is a fairly direct encounter in which the galaxies interpenetrate at first passage and material is strewn out to form a bridge between them. After several trials, the best fitting orbit was parabolic – in agreement with likely orbital geometrics from cosmological simulations (Benson 2005; Khochfar & Burkert 2006) – with a small perigalacticon of 1 kpc and both disks oriented nearly perpendicular to the orbital plane.

Snapshots of the stellar mass distribution, including three different projections of the remnant, at different stages of the encounter are shown in Figure 4. We treat the stellar particles as Bruzual & Charlot (2003) SSPs with ages and metallicities according to their formation time. Stars initialized with the progenitor disks are as-

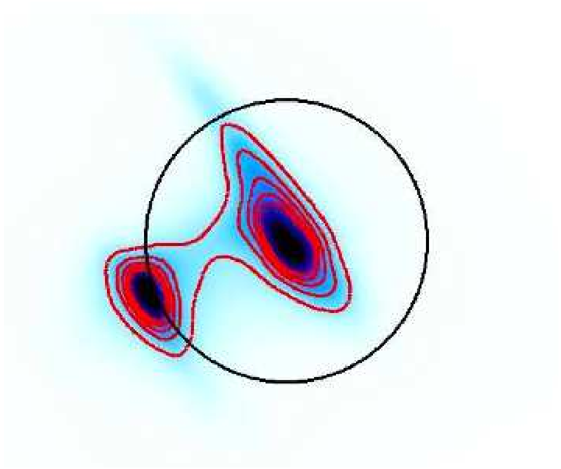

FIG. 5.— The rest–frame 1500Å surface brightness of the same snapshot in Figure 4, from the viewing angle that best matches the HDF–G4 system. This corresponds roughly to the observed i–band at $z = 4.42$. This image has the same scale and resolution as Figure 1, and has been convolved with the ACS PSF. The black circle, as in Figure 1, represents $1''$or 7 kpc projected physical separation, and the red contours show the isophotal shapes. Note that the simulations are able to roughly reproduce the rest–frame morphology of HDF–G4, with a bridge between the two components.

sumed to have formed 0.7 Gyr before the start of the simulation with low metallicity $Z = 1 \times 10^{-5}$. We neglect absorption and scattering by dust because the stellar population synthesis analysis in § 3 indicates that HDF–G4 is virtually dust–free. The best match to the observed optical morphology (rest–frame UV $\lambda \sim 1500$Å) of HDF–G4 was at $t = 0.17$ Gyr after the start of the simulation, and is shown in Figure 5. The snapshot shows the rest–frame $L_{1500\mathring{A}}$ surface brightness at the resolution of the observations in Figure 1 for $z = 4.42$, and convolved with the ACS PSF. The stellar mass at this snapshot is $2.9 \times 10^{10}\, M_\odot$ with a total SFR of 59 $M_\odot$ yr^{-1} ; both within the observational constraints given the uncertainty in the IMF and relative M/L ratios of C1 and C2. The synthetic SEDs of the two components over the physical scales in the ACS image, shown in Figure 6, are also a close match to the observations. Finally, the total luminosity from accretion onto the black hole is $L_{AGN} = 8 \times 10^8\, L_\odot$, which is well within the upper limit of $L_{AGN} < 2 \times 10^{10} L_\odot$ imposed by the observations. The ability of simulations to reproduce the observable features of this object supports our interpretation that HDF–G4 is an early–stage merger.

Finally, we note as a caveat that the isophotal shapes in Figure 5 are somewhat more elongated than those in the optical imaging data. Though our population synthesis modeling suggests that the overall effects of dust in the HDF–G4 system are small, because this is the rest–frame UV, even small amounts of dust in these elongations could substantially change their appearance in simulated observations. The structure of these features is also sensitive to the specific orbital geometry and the detailed structure of the progenitor disks, both of which may not be precisely captured in our modeling. The bridge, on the other hand, is produced by ram–pressure stripping of gas when the progenitors interpenetrate. Furthermore, if there were small amounts of dust in the system, this stripping would not necessarily carry the dust along with it. As a result, though the detailed isophotal shapes of the two components are sensitive to the initial conditions of our simulations, we believe that production of a UV–bright bridge between the two components is generic for any encounter with a small impact parameter, and is therefore the best evidence for an ongoing merger and the applicability of our modeling.

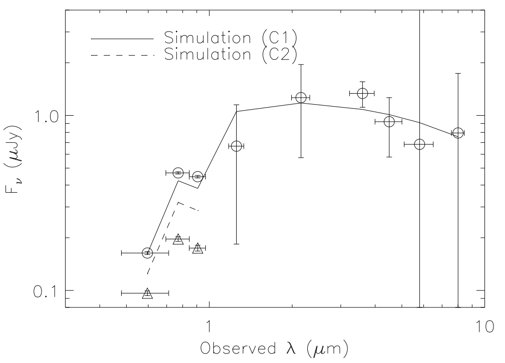

FIG. 6.— Simulated fluxes at $z = 4.42$ versus our observations of the HDF–G4 system for both components over the physical scales in the ACS image. The squares and solid line are the observed and simulated SED for C1, and the triangles and dashed line are the observed and simulated SED for C2.

5. DISCUSSION

In Figure 7, we use our simulation to predict the future evolution of the HDF–G4 system. This indicates that the two components will finally coalesce, with a peak in the starburst and AGN luminosity, around a redshift of $z \approx 3.5$. At this time, the HDF–G4 system will be a $L_{bol} \approx 4 \times 10^{11}\, L_\odot$ quasar. Based on the Hopkins et al. (2006a,c) quasar luminosity function models, we would expect there to be of order a couple such systems in the GOODS–North field. Although we cannot robustly constrain the space densities of these mergers, it is conservatively consistent with the expected counts.

Our simulations also suggest that by a redshift of $z \approx 2.5$, HDF–G4 will have a spheroidal morphology (see Figure 4), a stellar mass of $M_\star = 7.4 \times 10^{10}\, M_\odot$, and a SFR of 8.8 $M_\odot$ yr^{-1} ; a slowly star–forming but not entirely passive elliptical. Its colors will be red, with $(J - K)_{AB} \approx 1.2$, which is close to the color cut of $(J - K)_{AB} > 1.3$ for Distant Red Galaxies (DRGs: van Dokkum et al. 2003). The remnant also has a small effective radius – measured as in Cox et al. (2006) – relative to local spheroids of the same mass, with $R_e = 1.4 \pm 0.17$ kpc and an average inner stellar surface mass density within R_e of $\sigma_e = (0.6 \pm 0.03) \times 10^{10}\, M_\odot$ kpc^{-2}, where the errors take into account projection effects. This makes it similar to the compact, quiescent high redshift spheroids at $z \sim 2$ observed by Labbé et al. (2005) and Zirm et al. (2007), who find effective radii of $R_e \sim 0.5 - 1.1$ kpc, inner stellar surface mass densities of $\sigma_e \sim 0.7 - 4\, M_\odot$ kpc^{-2}, and stellar masses of $M_\star \sim 5 - 9 \times 10^{10}\, M_\odot$.

The existence of such an object further lends observational support to galaxy formation models which argue that mergers dominate the high-redshift buildup of spheroids and black holes (Hopkins et al. 2007d; Croton et al. 2006). It is difficult, on the other hand, to reconcile this with models which argue that spheroid and black hole formation at high redshift is driven by direct

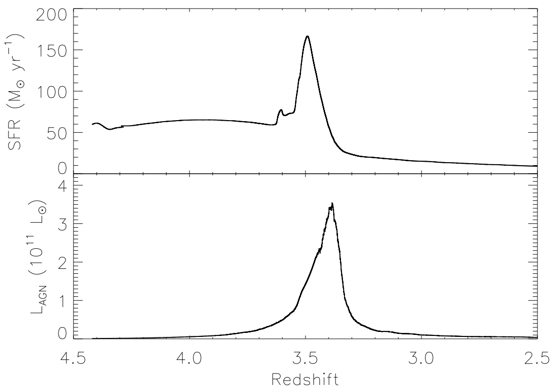

FIG. 7.— The future evolution of the SFR (top panel) and the AGN luminosity (top panel) of the HDF–G4 system as predicted by our simulations. This suggests that HDF–G4 will be a quasar at $z \approx 3.5$, and a quiescent spheroid at $z \approx 2.5$.

gas collapse/cooling (Granato et al. 2004) or disk instabilities (e.g., Bower et al. 2006). In the latter model, for example, mergers contribute only $\sim 0.1\%$ of bulge and BH growth at these redshifts, which would predict systems like HDF-G4 should be too rare to observe in small fields, should be already "dry" (i.e. spheroid-dominated, with much lower current SFRs), and should have pre-existing large BHs from their disk phase (given the disk masses and gas fractions necessarily present at these redshifts) which would, given gas is clearly still present (from the observed SFR), inescapably make the system a ($\sim 3 \times 10^{12}\, L_\odot$) quasar at the observed time. Therefore, it will be interesting to see if future observations of wider fields reveal HDF–G4 to be anomalous, or representative of a typical, albeit brief, phase of LBG evolution.

6. CONCLUSION

We present the rest–frame UV through NIR SED for HDF–G4, an interacting Lyman Break galaxy in GOODS-North with a spectroscopically confirmed redshift of $z = 4.42$ (Steidel et al. 1999), using data obtained from ACS, WIRCam, and IRAC. The two objects in this system – HDF–G4 and its previously unidentified companion – are both B_{435} band dropouts, have similar $V_{606} - i_{775}$ and $i_{775} - z_{850}$ colors, and are separated by $1''$, which at $z = 4.42$ corresponds to 7 kpc projected nuclear separation, and a bridge of material between them. We apply stellar population synthesis models (Bruzual & Charlot 2003) to the SED of HDF–G4, and find a best–fit population with solar metallically, an exponential star formation history, with e–folding time $\tau_0 = 440$ My, stellar age $\tau_\star = 720$ Myr, stellar mass $M_\star = 2.6 \times 10^{10} M_\odot$, and dust extinction $E(B-V) = 0$ with a reduced χ^2/d.o.f = 1.46. The observed stellar population, combined with the SED, system morphology, and projected nuclear separation, are used to constrain a model of the HDF–G4 system using a hydrodynamical simulation. This analysis suggests that HDF–G4 is the potential progenitor of a $z \approx 3.5$ quasar with $L \approx 4 \times 10^{11}\, L_\odot$, and a compact ($R_e = 1.4$ kpc) quiescent $z \sim 2.5$ spheroid consistent with the population observed by Labbé et al. (2005) and Zirm et al. (2007). Furthermore, the existence of such an object supports galaxy formation models in which major mergers drive the high redshift buildup of spheroids and black holes (e.g., Hopkins et al. 2007d).

We thank the referee for their helpful comments. This work is based on observations made with the *Spitzer* Space Telescope, which is operated by the Jet Propulsion Laboratory, California Institute of Technology, under NASA contact 1407. CFHT observations are supported through the Taiwan CosPA project.

REFERENCES

Adelberger, K. L., Steidel, C. C., Pettini, M., Shapley, A. E., Reddy, N. A., & Erb, D. K. 2005, ApJ, 619, 697

Ajiki, M., Taniguchi, Y., Fujita, S. S., Shioya, Y., Nagao, T., Murayama, T., Yamada, S., Umeda, K., & Komiyama, Y. 2003, AJ, 126, 2091

Alexander, D. M. et al. 2003, AJ, 126, 539

Barger, A. J., Cowie, L. L., & Richards, E. A. 2000, AJ, 119, 2092

Barmby, P. et al. 2004, ApJS, 154, 97

Benson, A. J. 2005, MNRAS, 358, 551

Bertin, E. & Arnouts, S. 1996, A&AS, 117, 393

Borys, C., Chapman, S., Halpern, M., & Scott, D. 2003, MNRAS, 344, 385

Bower, R. G., Benson, A. J., Malbon, R., Helly, J. C., Frenk, C. S., Baugh, C. M., Cole, S., & Lacey, C. G. 2006, MNRAS, 370, 645

Bruzual, G. & Charlot, S. 2003, MNRAS, 344, 1000

Calzetti, D. 2001, PASP, 113, 1449

Calzetti, D., Armus, L., Bohlin, R. C., Kinney, A. L., Koornneef, J., & Storchi-Bergmann, T. 2000, ApJ, 533, 682

Capak, P. et al. 2004, AJ, 127, 180

Chabrier, G. 2003, PASP, 115, 763

Chapman, S. C., Blain, A. W., Smail, I., & Ivison, R. J. 2005, ApJ, 622, 772

Coppin, K., Halpern, M., Scott, D., Borys, C., & Chapman, S. 2005, MNRAS, 357, 1022

Cox, T. J., Dutta, S. N., Di Matteo, T., Hernquist, L., Hopkins, P. F., Robertson, B., & Springel, V. 2006, ApJ, 650, 791

Croton, D. J. et al. 2006, MNRAS, 365, 11

Daddi, E., Cimatti, A., Renzini, A., Fontana, A., Mignoli, M., Pozzetti, L., Tozzi, P., & Zamorani, G. 2004, ApJ, 617, 746

Di Matteo, T., Springel, V., & Hernquist, L. 2005, Nature, 433, 604

Diolaiti, E., Bendinelli, O., Bonaccini, D., Close, L., Currie, D., & Parmeggiani, G. 2000, A&AS, 147, 335

Erb, D. K., Steidel, C. C., Shapley, A. E., Pettini, M., Reddy, N. A., & Adelberger, K. L. 2006, ApJ, 646, 107

Fazio, G. G. et al. 2004, ApJS, 154, 10

Franx, M. et al. 2003, ApJ, 587, L79

Giavalisco, M. et al. 2004, ApJ, 600, L93

Goldader, J. D., Goldader, D. L., Joseph, R. D., Doyon, R., & Sanders, D. B. 1997, AJ, 113, 1569

Granato, G. L., De Zotti, G., Silva, L., Bressan, A., & Danese, L. 2004, ApJ, 600, 580

Hopkins, P. F., Cox, T. J., Keres, D., & Hernquist, L. 2007a, ApJ, submitted

Hopkins, P. F., Hernquist, L., Cox, T. J., Di Matteo, T., Robertson, B., & Springel, V. 2006a, ApJS, 163, 1

Hopkins, P. F., Hernquist, L., Cox, T. J., & Keres, D. 2007b, ApJ, submitted

Hopkins, P. F., Hernquist, L., Cox, T. J., Robertson, B., Di Matteo, T., & Springel, V. 2006b, ApJ, 639, 700

Hopkins, P. F., Hernquist, L., Cox, T. J., Robertson, B., & Krause, E. 2007c, ApJ, submitted astro-ph/0701351

Hopkins, P. F., Richards, G. T., & Hernquist, L. 2007d, ApJ, 654, 731

Hopkins, P. F., Somerville, R. S., Hernquist, L., Cox, T. J., Robertson, B., & Li, Y. 2006c, ApJ, 652, 864

Hu, E. M., Cowie, L. L., Capak, P., McMahon, R. G., Hayashino, T., & Komiyama, Y. 2004, AJ, 127, 563

Huang, J. . et al. 2006, ArXiv Astrophysics e-prints

Ivison, R. J. et al. 2002, MNRAS, 337, 1

Kennicutt, Jr., R. C. 1998, ARA&A, 36, 189

Khochfar, S. & Burkert, A. 2006, A&A, 445, 403

Labbé, I. et al. 2005, ApJ, 624, L81

Lai, K., Huang, J.-S., Fazio, G., Cowie, L. L., Hu, E. M., & Kakazu, Y. 2007, ApJ, 655, 704

Law, D. R. et al. 2007, ApJ, 656, 1

Lotz, J. M., Madau, P., Giavalisco, M., Primack, J., & Ferguson, H. C. 2006, ApJ, 636, 592

Madau, P. 1995, ApJ, 441, 18

Madau, P., Pozzetti, L., & Dickinson, M. 1998, ApJ, 498, 106

Malhotra, S. & Rhoads, J. E. 2002, ApJ, 565, L71

Mobasher, B. et al. 2005, ApJ, 635, 832

Papovich, C., Dickinson, M., & Ferguson, H. C. 2001, ApJ, 559, 620

Peng, C. Y., Impey, C. D., Rix, H.-W., Kochanek, C. S., Keeton, C. R., Falco, E. E., Lehár, J., & McLeod, B. A. 2006, ApJ, 649, 616

Pettini, M., Kellogg, M., Steidel, C. C., Dickinson, M., Adelberger, K. L., & Giavalisco, M. 1998, ApJ, 508, 539

Rhoads, J. E. & Malhotra, S. 2001, ApJ, 563, L5

Rhoads, J. E. et al. 2005, ApJ, 621, 582

Richards, E. A. 2000, ApJ, 533, 611

Rigopoulou, D., Spoon, H. W. W., Genzel, R., Lutz, D., Moorwood, A. F. M., & Tran, Q. D. 1999, AJ, 118, 2625

Rigopoulou, D. et al. 2006, ApJ, 648, 81

Robertson, B., Hernquist, L., Cox, T. J., Di Matteo, T., Hopkins, P. F., Martini, P., & Springel, V. 2006, ApJ, 641, 90

Salpeter, E. E. 1955, ApJ, 121, 161

Sawicki, M. & Yee, H. K. C. 1998, AJ, 115, 1329

Scalo, J. M. 1986, Fundamentals of Cosmic Physics, 11, 1

Shapley, A. E., Steidel, C. C., Adelberger, K. L., Dickinson, M., Giavalisco, M., & Pettini, M. 2001, ApJ, 562, 95

Shapley, A. E., Steidel, C. C., Erb, D. K., Reddy, N. A., Adelberger, K. L., Pettini, M., Barmby, P., & Huang, J. 2005, ApJ, 626, 698

Shapley, A. E., Steidel, C. C., Pettini, M., & Adelberger, K. L. 2003, ApJ, 588, 65

Smail, I., Ivison, R. J., Owen, F. N., Blain, A. W., & Kneib, J.-P. 2000, ApJ, 528, 612

Springel, V. 2005, MNRAS, 364, 1105

Springel, V., Di Matteo, T., & Hernquist, L. 2005a, ApJ, 620, L79

—. 2005b, MNRAS, 361, 776

Steidel, C. C., Adelberger, K. L., Giavalisco, M., Dickinson, M., & Pettini, M. 1999, ApJ, 519, 1

Steidel, C. C., Adelberger, K. L., Shapley, A. E., Pettini, M., Dickinson, M., & Giavalisco, M. 2003, ApJ, 592, 728

Steidel, C. C. & Hamilton, D. 1993, AJ, 105, 2017

Surace, J. A., Sanders, D. B., & Evans, A. S. 2000, ApJ, 529, 170

Takeuchi, T. T. & Ishii, T. T. 2004, A&A, 426, 425

Taniguchi, Y. et al. 2005, PASJ, 57, 165

van Dokkum, P. G. et al. 2003, ApJ, 587, L83

Whitmore, B. C. & Schweizer, F. 1995, AJ, 109, 960

Yan, H., Dickinson, M., Giavalisco, M., Stern, D., Eisenhardt, P. R. M., & Ferguson, H. C. 2006, ApJ, 651, 24

Yan, H. et al. 2005, ApJ, 634, 109

Zirm, A. W., van der Wel, A., Franx, M., Labbé, I., Trujillo, I., van Dokkum, P., Toft, S., Daddi, E., Rudnick, G., Rix, H.-W., Röttgering, H. J. A., & van der Werf, P. 2007, ApJ, 656, 66